Investigations into modifications of neuromuscular physiology by axonal transport disruptions in *Drosophila* SOD1 mutants

Tristan C. D. G. O'Harrow[1]*, Atsushi Ueda[1]*, Xiaomin Xing[1*‡], Chun-Fang Wu[1]

[1] Department of Biology, University of Iowa, Iowa City, IA 52242, USA

* Equal contribution

‡ Current address: Department of Pharmacology, School of Medicine, University of California, Davis, CA, 95616

Abstract

Cu/Zn superoxide dismutase (SOD1) is a cytoplasmic antioxidant enzyme, which, when mutant in humans, is linked to familial cases of the motor neurodegenerative disease amyotrophic lateral sclerosis (ALS). The *Drosophila* SOD1 gene (*Sod*) shares a highly conserved sequence with the human homolog, and this study includes examinations of the established hypomorphic *n108* allele (Sod^{n108}), alongside a knock-in construct of the *G85R* allele found in human ALS patients (Sod^{G85R}). In addition to previously documented decreased adult lifespan and attenuated motor function, we show that *Sod* mutant *Drosophila* can display significant mortality during larval and pupal development. Immunostaining of neuronal membrane at neuromuscular synapses in *Sod* mutant larvae revealed presynaptic terminals of abnormal morphology, with incompletely segregated and enlarged synaptic boutons along the motor terminal branches, in which vital staining indicated mitochondrial aggregation. We demonstrate strong genetic interactions between Sod^{G85R} and the axon transport-linked *Pk* mutants Pk^{Pk} and Pk^{Sple} in larval NMJ morphology and neuromuscular transmission. Intracellular recordings of larval excitatory junction

potentials (EJPs) demonstrate enhanced EJP size in the double-mutant of Pk^{Pk} and Sod^{G85R}. To examine synaptic terminal excitability, maintained by Ca^{2+} channel action and independent of Na^{+} channel function, we used the Na_V blocker TTX, along with the K_V1 blocker 4-aminopyridine (4-AP) and the commonly used broad-spectrum K^{+} channel blocker tetraethylammonium (TEA). We were able to induce prolonged "plateau-like" EJPs, which were further extended in *Pk* mutants and *Pk*;*Sod* double-mutants. These observations were corroborated with focal EJP recording from individual boutons. Altogether, this study highlights alterations in synaptic morphology and function at a developmental stage prior to neurodegeneration and death of *Sod* mutant organisms, along with a potential role of axonal transport in the maintenance of neuronal health.

Introduction

The generation of reactive oxygen species (ROS) is a ubiquitous feature of energy metabolism in living cells. ROS are a class of free radicals that readily oxidize other molecules, and the resulting damage to cellular components over time is thought to be a normal feature of aging (Harman, 1956; Lushchak, 2014). The disruption of oxidative homeostasis that occurs as a result of increased ROS load is termed 'oxidative stress' (Paniker et al., 1970; Sies, 1997). While ROS have been implicated as signaling molecules in healthy physiological processes ranging from cell differentiation (Thannickal & Fanburg, 2000) to synaptic plasticity (Massaad & Klann, 2011), high oxidative stress predisposes proteins to misfolding (Berlett & Stadtman, 1997), lipids to peroxidation (Altan et al. 2003), and nucleic acids to breakage and mutation (Aitken & Krausz, 2001). Excessive oxidative stress has been implicated in neurodegenerative diseases, cardiovascular diseases, and cancer (Liguori et al., 2018; Uttara et al., 2009; Dhalla et al., 2000; Sosa et al., 2013). Both

53 eukaryotic and prokaryotic organisms produce antioxidant enzymes to maintain oxidative
54 homeostasis, including catalases, glutathione peroxidases, and superoxide dismutases
55 (Matés et al., 1999).
56
57 The antioxidant enzyme Cu/Zn superoxide dismutase (SOD1) forms homodimers that mainly
58 localize to the cytosol, and target superoxide molecules for neutralization (McCord &
59 Fridovich, 1969; Culotta & Daly, 2013). The reactions that SOD1 catalyzes sum to the
60 conversion of two superoxides (O_2^-) and two protons (H^+) to molecular oxygen (O_2) and
61 hydrogen peroxide (H_2O_2), which is targeted by the enzyme catalase for conversion into
62 molecular oxygen and water (O_2 & H_2O) (Mondola et al., 2016; Perry et al., 2010). The gene
63 encoding SOD1 is highly conserved across phyla, and both *Drosophila* and mice SOD1 null
64 mutants display reduced lifespans (Phillips et al., 1989; Zhang et al., 2016). Mutations in the
65 gene for SOD1 and decreased overall SOD1 activity have been found in some human
66 patients with the neurodegenerative disease amyotrophic lateral sclerosis (ALS), popularly
67 known as Lou Gehrig's disease or motor neuron disease (Rosen et al., 1993; Saccon et al.,
68 2013). ALS is a fatal neurodegenerative disease in humans, in which the gradual death of
69 motor neurons causes the muscles they innervate to weaken and atrophy (Rosen et al.,
70 1993; Rowland & Schneider, 2001; Galvin et al., 2017; Hardiman et al, 2011).
71
72 Generated by EMS mutagenesis, the *n108* allele of the *Drosophila* gene for SOD1 (*Sod*) has
73 been identified as a loss-of-function allele (Campbell et al., 1985, Phillips et al., 1989). Flies
74 homozygous for the *n108* allele (Sod^{n108}) display hypersensitivity to oxidative stress and
75 severely reduced lifespans. The *Drosophila G85R* allele (Sod^{G85R}) is a knock-in construct of
76 the missense allele of the same name found in human ALS patients (Şahin et al., 2017). The
77 *G85R* mutation site is conserved between the human and *Drosophila* genes, so the human
78 point mutation was introduced into the *Drosophila* gene by ends-out homologous

recombination. The G85R point mutation is in close proximity to a metal ion binding site that enables SOD1 to maintain structural stability. *Sod*^{G85R} homozygotes display locomotor defects as larvae, and near-full lethality at the pupal stage (Şahin et al., 2017).

The *Drosophila* larval NMJ (Jan & Jan, 1976; Atwood et al., 1993) is an excellent platform for the study of early motor synaptic characteristics that precede recognizable SOD1-linked neurodegeneration. Immunohistochemistry can make visible neuronal membrane and synaptic proteins at the NMJ. In particular, we used anti-horseradish peroxidase (anti-HRP: Jan & Jan, 1982) to view presynaptic terminal morphology, anti-Dlg (monoclonal antibody 4F3: Parnas et al., 2001) which also reveals subsynaptic reticulum (SSR) surround the synaptic boutons (Budnik et al., 1996), and the monoclonal antibody 22C10 (Fujita et al., 1982; Zipursky et al., 1984) to view the microtubule-associated protein Futsch that decorates mature microtubule structures (Hummel et al., 2000). We found that the presynaptic motor terminals of *Sod* mutant larvae carried enlarged synaptic boutons, which were also visible *in vivo* in our *Sod* mutant lines containing a cell membrane GFP (CD8-GFP: Lee & Luo, 2001) targeted to motor neurons (OK371-Gal4: Mahr & Aberle, 2006; C164-Gal4: Torroja et al., 1999) (Gal4-UAS system: Brand & Perrimon, 1993). Vital staining with the mitochondrial stain tetramethylrhodamine (TMRM) alongside presynaptic CD8-GFP revealed macropunctae, suggesting mitochondrial aggregation inside the enlarged boutons of *Sod* mutants. While it is known that mitochondria are important for Ca^{2+} buffering and ATP generation in the presynaptic terminal for synaptic transmission (MacAskill & Kittler, 2009), the extreme synaptic accumulation of mitochondria in *Sod* mutants may involve abnormal axonal transport. Indeed, our finding recapitulates aberrant mitochondrial distribution previously observed in human ALS patients and mouse models of ALS, with disrupted mitochondrial transport and morphology (De Vos et al., 2007; Ott et al., 2007; Smith et al., 2017; Vande Velde et al., 2011).

105

106 In *Drosophila*, the planar cell polarity gene *Prickle* (*Pk*) (Gubb & García-Bellido, 1982; Gubb
107 et al., 1999; Gray et al., 2011; Lin & Gubb, 2009; Tree et al., 2002) is expressed in the form
108 of the Pk^{Pk} (*Prickle Prickle*) and Pk^{Sple} (*Prickle Spiny-legs*) isoforms, and their mutants display
109 distinctly altered microtubule-mediated transport and microtubule dynamics in larval motor
110 axons, with related changes in neuronal excitability (Ehaideb et al., 2014; Ehaideb et al.,
111 2016). In this study, we employ mutants of both *Pk* isoforms to demonstrate strong
112 interactions with *Sod* in larval motor neuron synaptic morphology and neuromuscular
113 transmission.

114

115 Synaptic transmission at the NMJ can be analyzed with the method of recording excitatory
116 junction potentials (EJPs) with an intracellular electrode (Jan & Jan, 1976). Additionally, local
117 loose-patch recording of synaptic currents enables characterization of the contributions of
118 single synaptic boutons along the terminal branches to overall synaptic transmission (Renger
119 et al., 2000; Kurdyak et al., 1994) In this study we adopt the same recording configuration
120 with voltage recording of extracellular focal field potentials (efEJP, Xing & Wu, 2018a, b) to
121 infer the synaptic current flow underneath the pipette, an approach first established by Fatt
122 and Katz (1952) for analyzing miniature end-plate currents (mEPCs) and potentials (mEPPs)
123 at the frog neuromuscular junction. We were therefore able to correlate global intracellular
124 events and focal analysis of synaptic transmission.

125

126

127

128

129

130

131 **Materials and Methods**

132

133 Fly stocks

134 Flies and larvae were housed in bottles containing a cornmeal-agar medium (Frankel &
135 Brousseau, 1968), supplemented with 3g of yeast paste prepared as a 1:1 mixture of ddH_2O
136 and active dry yeast (Red Star Yeast Co., LLC). Flies were reared at a room temperature of
137 22 ± 1°C. The *Sod* mutants examined were those of alleles *n108* (Phillips et al., 1989) (gift
138 from John Phillips, University of Guelph, Ontario, Canada) and *G85R* (Şahin et al. 2017) (gift
139 from Barry Ganetzky, University of Wisconsin-Madison, USA). The wild-type control strain
140 used for Figures 1, 2, 3, and 4 was Canton-S (CS). For experiments in which a motor neuron
141 membrane tag was needed, the stock used carried a chr. II *UAS-CD8-GFP* recombined with
142 a chr. II motor neuron GAL4 driver (Brand & Perrimon, 1993), either *C164-Gal4* (Torroja et
143 al., 1999) or *OK371-Gal4* (Mahr and Aberle, 2006). The original recombined *OK371-Gal4*
144 *UAS-CD8-GFP* (*OK371::CD8-GFP*) was obtained from the National Centre for Biological
145 Sciences (Bangalore, Karnataka, India). *Sod* lines used to produce the data represented in
146 Figure 1 were balanced over a TM6 balancer with a dominant *Tubby* (*Tb*) marker (TM6, *Tb*).
147 The Pk^{Pk} and Pk^{Sple} lines used in this study have been documented previously (Ehaideb et
148 al., 2014). The wild-type control strain used for Figure 5 was the Oregon-R (OR) used in
149 Ehaideb et al. (2014). All *Pk;Sod* double-mutant lines were generated in the Wu lab by
150 conventional genetic crosses.

151

152 Developmental lethality studies

153 Housing and medium conditions for the developmental lethality study (Figure 1) were
154 identical to those described in the main "Fly stocks" section. Flies including 20-40 females
155 were used to seed each bottle. Counts of deaths and eclosions were performed 16-17 d.
156 after seeding. The TM6, *Tb* balancer carried by *Sod* heterozygous wandering 3rd instar

157 larvae and pupae was used to distinguish them from *Sod* mutant homozygotes. Dead larvae
158 appear as darkened corpses on the wall of the housing bottle. Dead pupae were entirely
159 black, or contained a mixture of dark and empty patches, as confirmed by transmitted light
160 under a dissection scope. Juvenile flies dead during eclosion were distinguished from flies in
161 the process of eclosing by a second observation 15-30 min after the first. Juvenile fly corpses
162 were also frequently darker than their live counterparts.
163
164 Larval preparations, vital staining, & immunohistochemistry
165 Wandering third instar larvae were dissected, as per the "fillet preparation method", in HL 3.1
166 saline (Feng et al., 2004). HL3.1 used in immunohistochemistry or vital staining experiments
167 contained 0.1 mM Ca^{2+}. Tetramethylrhodamine (TMRM, $C_{25}H_{25}ClN_2O_7$) (Floryk & Houštěk,
168 1999) vital staining of larval preps for mitochondria was done at 100 nM in HL 3.1 for 20
169 minutes (in a light-impermeable chamber to prevent TMRM photobleaching), after which the
170 bath was replaced with TMRM-free HL 3.1 before microscopy. Before antibody staining,
171 larval preps were fixed in 3.7% formaldehyde in HL 3.1 for 25-30 minutes. Fixed preps were
172 incubated with an FITC-conjugated goat antibody to HRP at 1:50 in phosphate buffer saline,
173 at 4°C for 12-48 h. Anti-HRP (Jan & Jan, 1982) recognizes a neural carbohydrate antigen in
174 *Drosophila* (Kurosaka et al., 1991). For double-staining with anti-HRP and anti-Dlg
175 (monoclonal AB 4F3: Parnas et al., 2001) or anti-Futsch (monoclonal AB 22C10: Fujita et al.,
176 1982; Zipursky et al., 1984) staining, fixed larval preps were incubated with the primary
177 monoclonal AB at 1:100 in phosphate buffer saline, at 4°C for 12-48 h, rinsed, and incubated
178 in phosphate buffer saline containing anti-HRP(conj. FITC) and a secondary TRITC-
179 conjugated anti-mouse IgG antibody, both at 1:50. The 4F3 and 22C10 antibodies were
180 obtained from the Developmental Studies Hybridoma Bank (DSHB) (University of Iowa, Iowa
181 City, IA, USA). The FITC-conjugated anti-HRP and TRITC-conjugated anti-mouse IgG were
182 obtained from Jackson ImmunoResearch Laboratories (West Grove, PA, USA). Larval NMJ

183 images, vital and fixed, were gathered on a Leica DM IL LED inverted microscope (Leica
184 Microsystems Inc., Buffalo Grove, IL, USA), using the Leica Application Suite X software.
185
186 Larval NMJ morphology and mitochondrial distributions
187 Examination of *Sod* single-mutant NMJ morphology (Figure 2) was carried out in muscles 4
188 (M4) and 13 (M13), in abdominal segments A3, A4, and A5, and quantifications from the
189 different segments were pooled. Examination of *Pk;Sod* double-mutant NMJ morphology
190 (Figure 4) was carried out in muscle 4 (M4) in abdominal segments A2, A4, and A6, and
191 quantifications from the different segments were pooled. Counts of boutons from M4 include
192 only type Ib boutons. Ib and Is boutons and branches in M13 were quantified separately.
193 Counts of specific bouton morphologies ("unsegregated" boutons and large terminal boutons)
194 are from M4 (Ib). For branch counting, a branch was defined as a terminal process carrying
195 at least two boutons (Zhong et al., 1992). A bouton was described as incompletely
196 segregated ("unsegregated") if the width of the narrowest point on the neck preceding it was
197 greater than 80% of the width of the widest point on the bouton. If multiple unsegregated
198 boutons appeared in a row, it could be difficult count them. In these cases, counts were
199 conservative. A terminal bouton was determined to be the "largest" if it was measurably
200 larger than any other bouton on that branch, past the last branching point.
201
202 Photography of NMJ mitochondria was completed within 30 minutes after TMRM
203 mitochondrial staining to mitigate effects of post-dissection physiological decline on results.
204 Counts of putative mitochondrial aggregates in enlarged terminal boutons were obtained
205 from larvae in which the NMJ membrane carried CD8-GFP driven by C164-Gal4 or OK371-
206 Gal4, making bouton morphology visible in the green fluorescence channel during vital
207 staining in the red channel.
208

209 Electrophysiology

210 All electrophysiological recordings were based on published protocols, and performed in
211 HL3.1 saline (Feng et al., 2004) (Composition (mM): 70 NaCl, 5 KCl, 0.1 $CaCl_2$, 4 $MgCl_2$, 10
212 $NaHCO_3$, 5 trehalose, 115 sucrose, 5 HEPES) (pH adjusted to 7.1). Intracellular recording of
213 excitatory junction potentials (EJPs) was adapted from Ueda and Wu (2006). Recording of
214 extracellular focal EJPs (efEJPs) was shown in Ueda and Wu (2009) and Xing and Wu
215 (2018a,b). For nerve-evoked action potentials, 0.1 ms stimuli were applied to the cut end of
216 the segmental nerve through a suction pipette. To enable analysis of presynaptic terminal
217 excitability, we also performed electrotonic stimulation (Wu et al., 1978; Ganetzky & Wu,
218 1982; 1983). Briefly: Tetrodotoxin (TTX) was applied to block Na+ channels. To achieve
219 direct electrotonic stimulation of the terminal, a 1 ms stimulus was applied to the cut
220 segmental nerve, which was sucked into the stimulation electrode, nearly up to the entry
221 point into the muscle, so as to allow the stimulus to passively propagate to the terminal and
222 depolarize the endplate membrane (Lee et al., 2014). In this manner, CaV channels
223 were directly triggered by local depolarization, independent from invasion of axonal Na+
224 action potentials. Further, a significant portion of multiple K+ channel species, including
225 *Shaker* (Kv1), were blocked by co-application of 4-aminopyridine (4-AP) and
226 tetraethylammonium (TEA) (Jan & Jan, 1977; Singh & Wu, 1999). Electrotonic stimulation of
227 the larval NMJ with TTX, 4-AP, and TEA has been shown in Lee et al. (2014). Such
228 manipulations allow for the examination of terminal excitability driven by Ca2+ channels with
229 reduced repolarization regulation by a range of K+ channels, with the exclusion of axonal
230 potential interplay.

231

232 Statistics

233 Overall distributions of deaths throughout the lifecycle (Figure 1) were compared using
234 Fisher's exact test. Counts of NMJ boutons and branches and of enlarged terminal and

unsegregated boutons (Figures 2 and 3) were examined with Kruskal-Wallis testing between all groups within muscle # and parameter (eg. M4, boutons), followed by rank-sum (Mann-Whitney U) post hoc between individual groups. EJP sizes were compared with one-way ANOVA (Figure 4B). Plateau-like EJP durations were compared by F-test (Figure 4D). Counts of NMJ mitochondrial macropunctae (Figure 6) were compared with Kruskal-Wallis testing followed by rank-sum (Mann-Whitney U) post hoc.

Results

<u>Lethality of *Sod* mutants during different developmental stages</u>

During fly husbandry and maintenance of fly stocks, we observed striking mortality during the development of Sod mutants. We therefore proceeded with a systematic study, comparing mortality rates at different developmental stages in Sod^{n108} and Sod^{G85R}. The mortality rates recorded refer to percentages of the total number (n = 150 - 360) of individuals counted at all stages (Figure 1C). *Drosophila* of the wild-type strain *Canton-S* exhibited no death at the wandering 3rd instar larval stage, a low rate of 3% mortality during pupal development, and no death due to unsuccessful eclosion (Figure 1C). In contrast, homozygotes from both *Sod* mutant lines studied displayed clear lethality during development, that differed significantly from WT ($p < 0.001$). *n108* and *G85R* 3rd instar larvae died at similar rates, of approx. 7% and 8%, respectively, but the phenotypes diverge at the pupal stage. In the the loss-of-function *n108* mutant, 10% of individuals died during the pupal stage, but nearly all pupae of the ALS-linked *G85R* allele died before eclosion (~91% of individuals). 1 out of 210 *G85R* individuals made it into eclosion, however it died in the process. 43% of *n108* individuals died during the eclosion process, and the remaining 40% successfully eclosed as juvenile adults. The mortality patterns of the balanced heterozygotes (*Sod/TM6,Tb*) did not differ significantly

261 from WT, as none of them displayed larval death or death at eclosion, and none had a pupal
262 death rate above 4% (WT rate: 3%), indicating no dominant or semi-dominant developmental
263 mortality in *Sod* mutants.
264
265 Altered larval neuromuscular junction morphology
266 The *Sod* mutants displayed mild alterations in NMJ outgrowth, that were readily visible in
267 counts of boutons per NMJ (Figure 2B). Counts of Ib branches and boutons in M4 and M13
268 in *G85R* yielded distributions that were not significantly different from WT. While the increase
269 in *G85R* M13 Is branches was nonsignificant, the numbers of Is boutons were significantly
270 increased compared to WT ($p < 0.05$). NMJ outgrowth was increased in *n108* compared to
271 WT, with more more Ib boutons in M4 ($p < 0.05$) and M13 ($p < 0.001$), more Ib branches on
272 M13 ($p < 0.01$), and a visible but nonsignificant increase in numbers of M4 Ib branches
273 (Figure 2B). Where *n108* NMJ complexity was significantly greater than WT, it was also
274 significantly increased compared to *G85R*, indicating physiological differences between
275 mutants with the loss-of-function allele and those with the ALS-linked allele.
276 Both *Sod* mutants displayed increases in numbers of unsegregated boutons per M4 Ib
277 branch compared to WT (*G85R*: $p < 0.001$, *n108*: $p < 0.05$) (Figure 2C). Similarly, terminal
278 boutons that were enlarged compared to other boutons on the same M4 Ib branch appeared
279 more frequently in both *Sod* mutants than in WT (*G85R*: $p < 0.001$, *n108*: $p < 0.01$) (Figure
280 2C).
281
282 Unlike the *Sod* single-mutants, phenotypes of NMJ complexity (M4, Ib) in Pk^{Pk}, Pk^{Sple}, and
283 their double mutants with *G85R* were most visible in changes to the numbers of branches
284 per NMJ. Compared to WT, Pk^{Pk};*G85R* displayed significantly more boutons ($p < 0.01$), and
285 Pk^{Sple};*G85R* displayed significantly fewer ($p < 0.01$). Both double-mutants displayed fewer
286 branches than either corresponding *Pk* single-mutant (both $p < 0.001$), and Pk^{Sple};*G85R*

287 displayed a number of boutons similar to the *G85R* single-mutant, strikingly fewer than the
288 Pk^{Sple} single-mutant. ($p < 0.001$). Both *Pk* single-mutants displayed slightly more boutons
289 than WT (both $p < 0.05$). None of the *Pk* single-mutants or *Pk*;*G85R* double-mutants
290 displayed a number of unsegregated boutons that was significantly different from WT, nor
291 was there a clear difference between WT and the *Pk* single-mutants in the rate at which
292 terminal boutons were enlarged. However, both *Pk*;*G85R* double-mutants displayed enlarged
293 terminal boutons at rates lower than *G85R*, but still greater than WT (both $p < 0.01$).
294
295 <u>Genetic interaction between *Sod* and *Pk* in motor neuron excitability and synaptic</u>
296 <u>transmission</u>
297 In light of the NMJ morphological defects manifested in *Sod* through its interaction with *Pk*
298 mutations, we examined neuromuscular transmission for related defects. When the motor
299 axon bundle was stimulated with 0.1 ms pulses in HL3.1 saline containing 0.2 mM Ca2+, we
300 detected reliable EJP responses in *Sod* and *Pk* mutant larvae. In *Sod* mutants (hypomorphic
301 alleles *n108* and *x39*/*n108*, as well as the ALS-related *G85R* allele), EJP response upon
302 nerve stimulation was similar to that in WT ($p > 0.05$, Figure 4B). EJP size in the *Pk* alleles of
303 *Pk* (*Pk1* and *Pk30*, data combined in Figure 4) was comparable to WT, while EJP size was
304 significantly decreased in the mutants of the *Sple* allele ($p<0.05$, One-Way ANOVA).
305 However, the double-mutant Pk^{Pk1};Sod^{G85R} showed unusually large EJPs (Figure 4B, $p <$
306 0.05, One-Way ANOVA). Abnormal synaptic transmission can be attributed to alterations in
307 ion channels participating in regulation of presynaptic terminal membrane depolarization to
308 control Ca^{2+} influx that triggers release of synaptic vesicles from presynaptic terminals.
309
310 We examined potential alterations of ionic mechanisms using a previously established
311 protocol of direct electrotonic stimulation of the axon terminal, after silencing the axon Na+
312 spikes via TTX (Ganetzky & Wu, 1982, 1983; Ueda & Wu 2009; Lee et al., 2013). We also

313 removed the repolarization force via K+ channel blockers, 4-AP and TEA. 4-AP specifically
314 blocks rapidly inactivating A-current (K_v1, *Shaker* channels) and TEA reduces a broad range
315 of K+ currents (Jan & Jan, 1977). The axon terminal was depolarized by electrotonic spread
316 of a stimulus of increased duration (1 ms, see Methods), in HL3.1 saline containing 0.1 mM
317 Ca2+. Under this condition, we observed strikingly prolonged EJPs, with durations up to a
318 few seconds, that reflected transmitter release triggered by sustained presynaptic Ca2+
319 action potentials (Ca_V2, *cac*: Smith et al., 1996; Kawasaki et al., 2002; Lee et al., 2014)
320 (Figure 4C) (Ueda & Wu, 2009). This observation is consistent with electrotonically-triggered
321 prolonged regenerative postsynaptic potentials first described in the squid giant synapse and
322 the frog NMJ (Katz & Miledi, 1967a,b). Our results showed that, in fact, such prolonged
323 plateau-like EJPs were enhanced in both the Pk^{Pk} and Pk^{Sple} mutants despite the decreased
324 baseline transmission in Pk^{Sple} and WT-like transmission in Pk^{Pk} (Figure 4B). Sod mutation
325 alone did not affect the plateau EJPs, but Pk^{Pk};Sod^{G85R} showed prolonged plateau EJPs,
326 suggesting a complex *Sod-Pk* mutant interaction. The previously reported dominant effect of
327 Pk^{Pk} (Ehaideb et al., 2014) was also confirmed when we observed explosive efEJPs in the
328 double mutant Pk^{Pk}/+;Sod^{n108} (Supplemental Figure 1).
329
330 Extracellular focal recordings of miniature end-plate potentials (mEPPs) generated by
331 individual releasing sites have been described in the frog neuromuscular junction by Fatt &
332 Katz (1952). In our study, the focal extracellular field potentials (extracellular focal EJPs or
333 efEJPs) corresponding to the explosive events were collected to compare with the
334 intracellularly recorded plateau-like potentials. Under the same conditions used to record
335 plateau-like EJPs intracellularly (TTX + 4-AP + TEA, 0.1 Ca2+, 1 ms stimuli), a glass
336 electrode with an opening approx. 7-10 μm was placed on the NMJ of muscles 6 and 7 (see
337 Methods) in an attempt to record local field potentials) generated mainly by a single bouton,
338 with some contributions from neighboring boutons (Figure 5). In fact, we recorded prolonged

synaptic activities with waveforms of long durations consistent with our intracellular recordings, but with different complex waveforms. Since the focal recording of the potentials generated by synaptic currents, the plateau potentials observed extracellularly reflects local muscle membrane potentials that necessarily change the driving force for the local synaptic currents (the difference between the membrane potential and equilibrium potential for the glutamate receptor current, that is nearly 0 (Jan & Jan, 1976; Stewart et al., 1994; Kurdyak et al., 1994). Therefore, the efEJPs collected during the plateau-like EJPs are not strictly proportional to the amount of transmitter release. Our results suggest a synergistic effect between sod and pk alleles in controlling the excitability of presynaptic terminals, which was governed by the local expression of Ca2+ and K+ channels.

<u>Disrupted mitochondrial distribution at the larval NMJ</u>

Mitochondrial staining with TMRM of the larval NMJ in Sod^{G85R} reared at RT revealed brightly stained "macropunctae"(Figure 6A) in over half (52%) of all terminal boutons compared to just 11% in WT and 16% in Sod^{n108} (both $p < 0.001$ compared to Sod^{G85R}) (Figure 6B). Bright spots are in contrast to the dimmer and more diffuse staining seen in most WT and Sod^{n108} NMJs. In larvae expressing GFP targeted to motor neuron membrane (UAS-CD8-GFP under the control of OK371-Gal4 or C164-Gal4), an association between synaptic bouton morphology and the presence of mitochondrial aggregates became apparent in both WT and Sod^{G85R} (Figure 6C). Of terminal boutons that were enlarged relative to other boutons in the branch (Figure 2A), 53% in WT and 77% in Sod^{G85R} contained TMRM macropunctae. In contrast, only 12% of WT and 32% of Sod^{G85R} boutons that were not relatively enlarged were stained with macropunctae.

365 **Discussion**

366

367 Our study contrasts the loss-of-function *n108* allele of *Sod* with the ALS-linked *G85R* allele,
368 by demonstrating clear differences in the developmental stages at which the mutants of each
369 allele die. The contrast is further enhanced by differences between their neuromuscular
370 synapse morphologies. We found potential mechanistic links between abnormal distribution
371 of mitochondria in Sod^{G85R} and synaptic bouton enlargement, consistent with the striking
372 interaction with *Pk*, known to affect axonal transport. Further, following pharmacological
373 blockade of Na+ and K+ currents in our electrophysiological experiments, the remaining
374 Ca2+ currents appeared to initiate more physiological actions, further enhanced in *Pk*
375 mutants and *Pk*;*Sod* double-mutants.

376

377 <u>Developmental death in *Sod* mutants</u>

378 This study of *Drosophila Sod* mutant lethality extends specificity and aspects of mutational
379 effects on the developmental stages in which deaths occur. Specifically, we distinguish
380 between death of the fully developed juvenile fly during eclosion from the pupal casing, and
381 death mid-pupal development, which is characterized by a pupal casing that remains closed.
382 As a result, we established allele-dependent developmental lethality phenotypes. The *n108*
383 lethality occurs largely during eclosion and may be due to physical weakness of the juvenile.
384 The vast majority of *G85R* death occurs during pupal development, often prior to formation of
385 adult morphology, as seen by a lack of red adult eyes visible through the pupal casing of
386 late-stage pupae (Bainbridge & Bownes, 1981).

387

388 <u>Aberrant NMJ morphology and physiology</u>

389 Overgrowth of the Sod^{n108} NMJ has been documented previously, and another oxidative
390 stress-sensitive mutant (*spinster*) was shown to have similar overgrowth. Further, the two

391 genes show synergistic interactions (Milton et al., 2011). Our result also demonstrated
392 overgrowth in *n108* Ib tonic synapses, but this did not hold true for Is phasic synapses. The
393 *G85R* larval NMJ has also been characterized (Held et al., 2019) although the bouton
394 number did not seem to differ significantly from their control. In this study, we also found no
395 clear difference in bouton numbers, but striking bouton morphological alterations could be
396 demonstrated in *G85R* larvae (Figure 2A). Additional immunostaining of proteins constituting
397 the presynaptic machinery, such as synaptotagmin and dynamin (Estes et al., 1996), or
398 postsynaptic elements such as glutamate receptors (Harris & Littleton, 2015), could elucidate
399 the functional relevance of the unusual bouton morphologies in *Sod* mutants.
400
401 We found similarly increased NMJ outgrowth in Pk^{Sple} and Pk^{Pk}. The increased NMJ
402 outgrowth observed in the Pk^{Sple} single-mutant may be related to its previously reported
403 increased neuronal excitability (Ehaideb et al., 2014). Other hyperexcitable mutants, such as
404 the double-mutant of K^+ channel mutants *Shaker* and *eag*, also exhibit significant NMJ
405 overgrowth (Zhong et al., 1992). The similarly increased outgrowth in Pk^{Pk} is in spite of a lack
406 of previously documented hyperexcitability. However, our electrophysiological studies with
407 electrotonic stimulation under blockade of Na+ channels (TTX) and K+ channels (4-AP &
408 TEA) revealed plateau-like potentials *Pk* and *Pk*;*Sod* mutants. These long potentials may be
409 driven by the action of the Ca2+ channel *cacophony* (*cac*), as these waveforms are
410 suppressed by mutation of *cac* (Lee et al., 2013) and application of Co2+, which blocks Ca2+
411 channels (Ueda & Wu, 2009). The extended plateau-like potentials in *Pk* and *Pk*;*Sod* could
412 therefore reflect a joint effect, with extended Ca2+ channel currents. The reduced transport
413 (Ehaideb et al., 2014) in Pk^{Pk} may affect local channel distributions, which could in turn alter
414 ion currents. Furthermore, Pk has been reported to physically interact with Synapsin1
415 (Paemka et al., 2013), and consequences of an interaction between *Sod* and *Pk* may
416 therefore involve Synapsin1 (Klagges et al., 1996) function, which influences synaptic

417 development (Vasin et al., 2014), and synaptic vesicle formation and release (Akbergenova
418 & Bykhovskaia, 2007).
419
420 The outgrowth of $Pk^{Pk};Sod^{G85R}$ between the levels of Pk^{Pk} and Sod^{G85R} resembles an
421 averaging effect. $Pk^{Sple};Sod^{G85R}$ exhibits an even simpler NMJ morphology than Sod^{G85R} in
422 spite of the increased outgrowth in Pk^{Sple}, demonstrating an unexpected undergrowth
423 phenotype associated with the genetic interaction. Additionally, the plateau-like EJPs we
424 observed under Na+ and K+ channel blockade appear in $Pk^{Pk};Sod^{G85R}$ and $Pk^{Sple};Sod^{G85R}$. *Pk*
425 apparently interacts with *Sod* in a dominant manner, because Pk^{Pk}/+ and *Sod*
426 (Pk^{Pk}/+;Sod^{n108}/Sod^{n108}) produced a strong effect on synaptic transmission, comparable to
427 $Pk^{Pk};Sod^{G85R}$ (Supplementary Figure 1).
428
429 <u>Mitochondrial aggregation associated with bouton morphology</u>
430 The brightly TMRM-stained NMJ boutons in Sod^{G85R} could reach several-fold, within the
431 resolution of the fluorescent microscopy, the increased signal may reflect accumulated
432 mitochondria. These potential mitochondrial aggregates could be related to dysfunctional
433 transport, which has previously been reported in SOD1-based models of ALS (Bilsland et al.,
434 2010; De Vos et al., 2007). Transport disruption could also contribute to the bouton
435 enlargement we found appeared to be linked to bright mitochondrial staining. Due to the
436 mechanics of TMRM, which is pulled into mitochondria by membrane potential (Floryk &
437 Houštěk, 1999), it remains to be further explored whether the brightly stained
438 "macropunctae" we identified reflect mitochondria of higher membrane potential, increased
439 mitochondrial volume, or a combination of the two.
440
441 Mutant SOD1 is the most commonly identifiable risk factor in human patients with familial
442 ALS (Zarei et al., 2015). By exploiting the amenability of the *Drosophila* larval neuromuscular

443 preparation to the study of motor synapses at an early developmental stage, we detect clear
444 signs of synaptic physiology and morphology alterations in *Sod* mutants. Additionally,
445 abnormal distributions of synaptic mitochondria in *Sod,* and severe NMJ phenotypes in *Sod*
446 double-mutants with transport-affecting *Pk* mutations, suggest dysfunctional transport may
447 contribute to early SOD1-linked pathology. Our work therefore contributes to documentation
448 of phenotypes and potential mechanisms that may facilitate future studies to uncover critical
449 events leading to irreversible and terminal motor neuron degeneration in ALS.

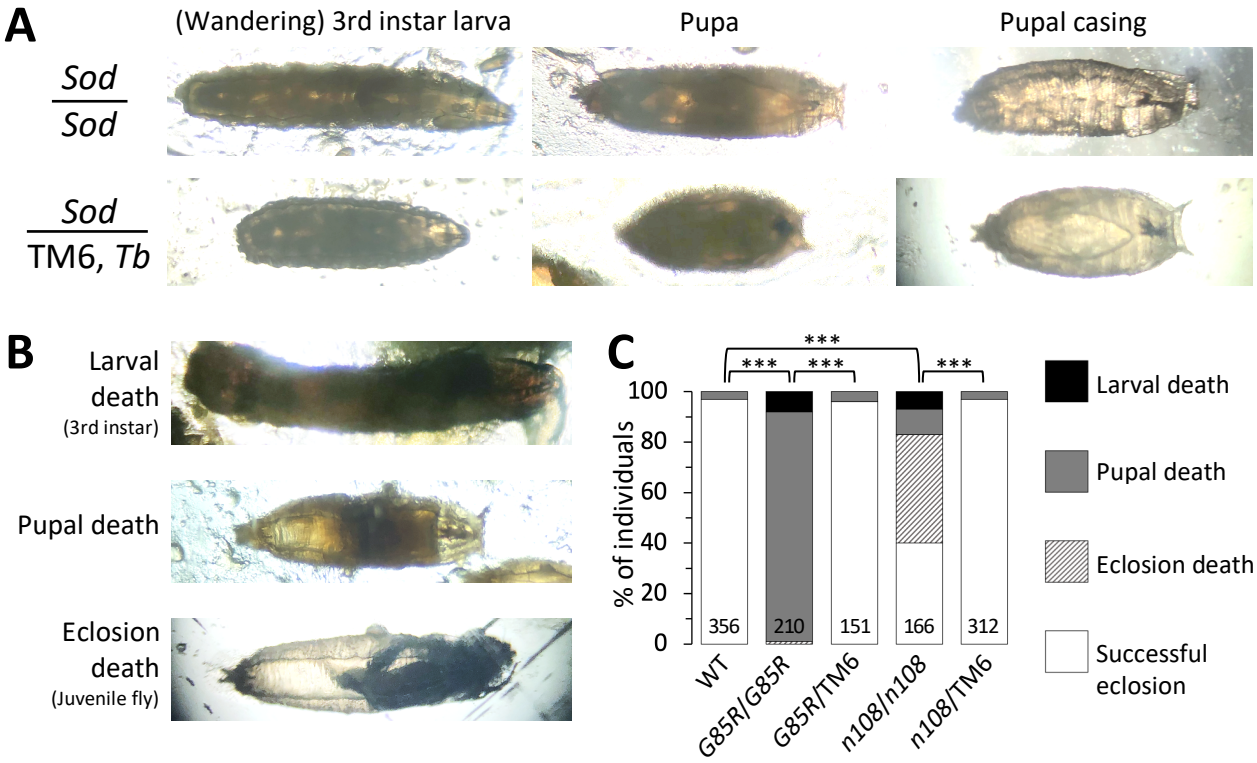
A
(Wandering) 3rd instar larva
Pupa
Pupal casing
Sod / Sod
Sod / TM6, Tb
B
Larval death (3rd instar)
Pupal death
Eclosion death (Juvenile fly)
C
% of individuals
100
80
60
40
20
0
356
210
151
166
312
WT
G85R/G85R
G85R/TM6
n108/n108
n108/TM6
***
Larval death
Pupal death
Eclosion death
Successful eclosion

Figure 1. Developmental lethality in *Sod* mutants.

(A) Representative images of larvae, pupae, and empty pupal casings of *Sod* mutant homozygotes (*Sod*/*Sod*) and balanced heterozygotes (*Sod*/TM6, *Tb*). *Sod* homozygotes have wild-type body morphology, and the TM6 balancer granted the heterozygotes shorter and fatter *Tubby* (*Tb*) body shape. The larvae represented are specifically of the wandering 3rd instar stage, immediately pre-pupation. Empty pupal casings are left over after successful eclosion of the juvenile fly.

(B) Images of *Sod* homozygotes dead during the wandering 3rd instar larval, pupal, or eclosion stages. Dead larvae are identifiable by their immobility and dark color and dead pupae have unevenly distributed contents and dark patches. Juvenile flies dead during eclosion were distinguished from flies in the process of eclosing by a second observation 15-30 min after the first. Juvenile fly corpses were also frequently darker than their live counterparts.

(C) Rates of lethality during development in wild-type (WT), Sod^{G85R} (*G85R*/*G85R*), Sod^{G85R}/TM6,*Tb* (*G85R*/TM6), Sod^{n108} (*n108*/ *n108*), and Sod^{n108}/TM6,*Tb* (*n108*/TM6). Dead individuals were counted at the 3rd instar larval stage (black), pupal stage (solid gray), and eclosion (gray stripes). Rates of successful eclosions (white) are from counts of empty pupal casings. *** indicates $p < 0.001$ (Fisher's exact test). *n* of individuals are indicated at the bottom of each bar.

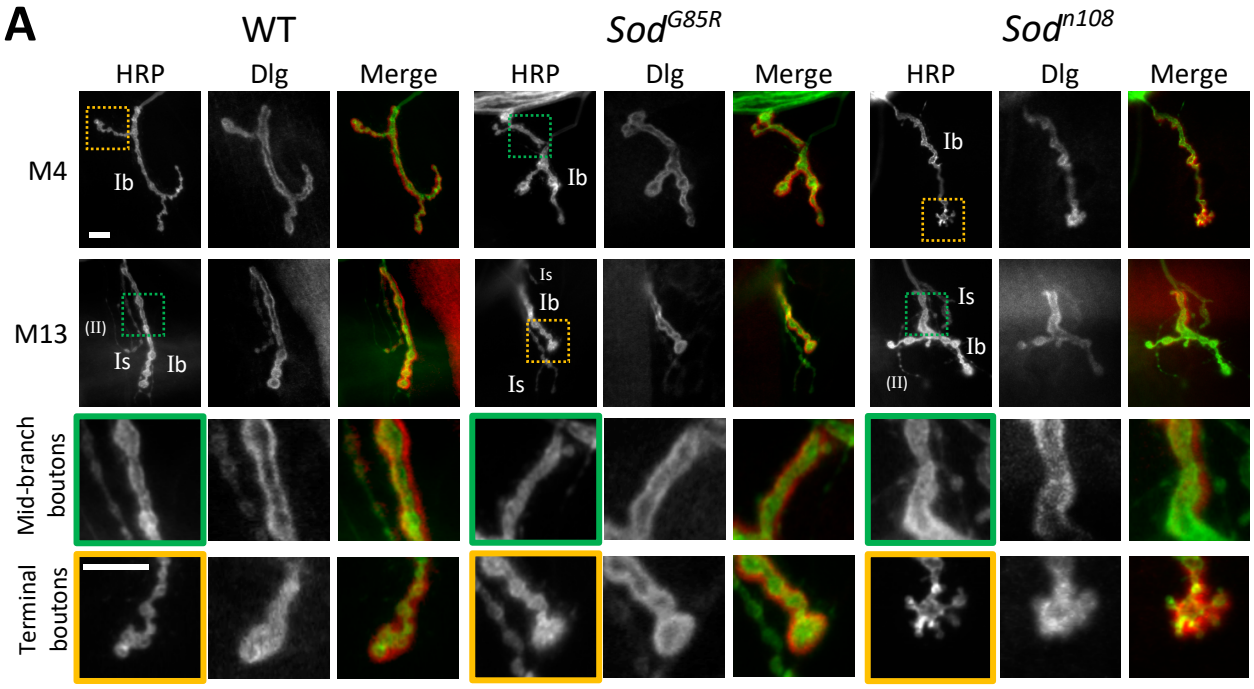
A
WT
Sod^G85R
Sod^n108
HRP
Dlg
Merge
M4
M13
Ib
Is
(II)
Mid-branch boutons
Terminal boutons

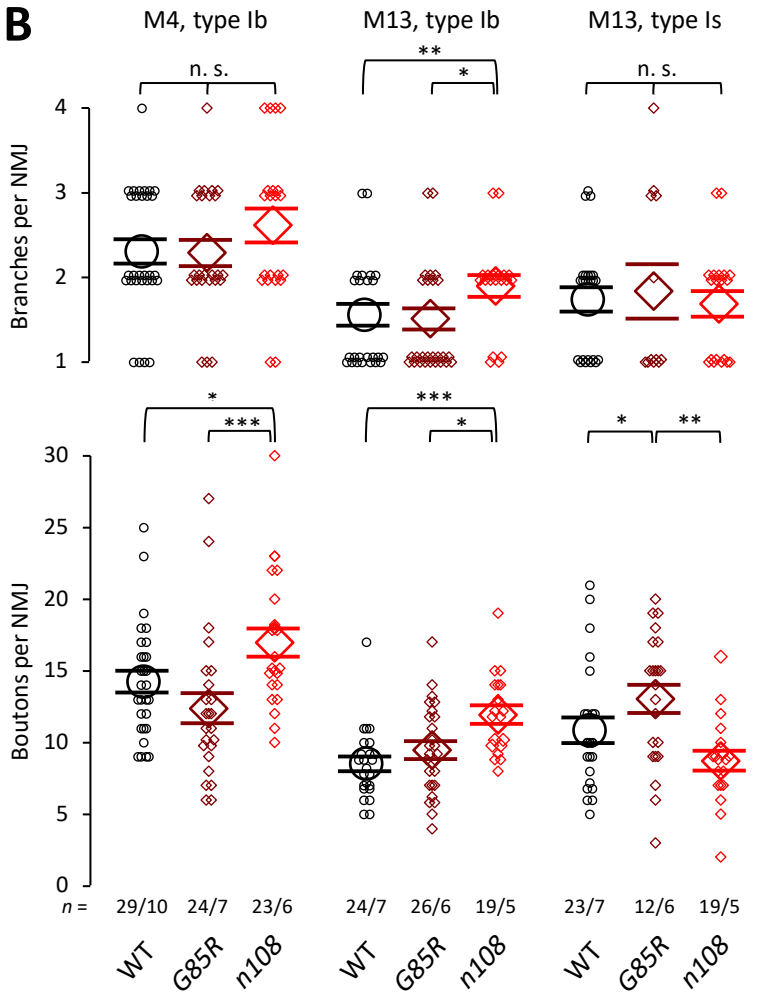
B
M4, type Ib
M13, type Ib
M13, type Is
n. s.
Branches per NMJ
Boutons per NMJ
n =
29/10
24/7
23/6
24/7
26/6
19/5
23/7
12/6
19/5
WT
G85R
n108

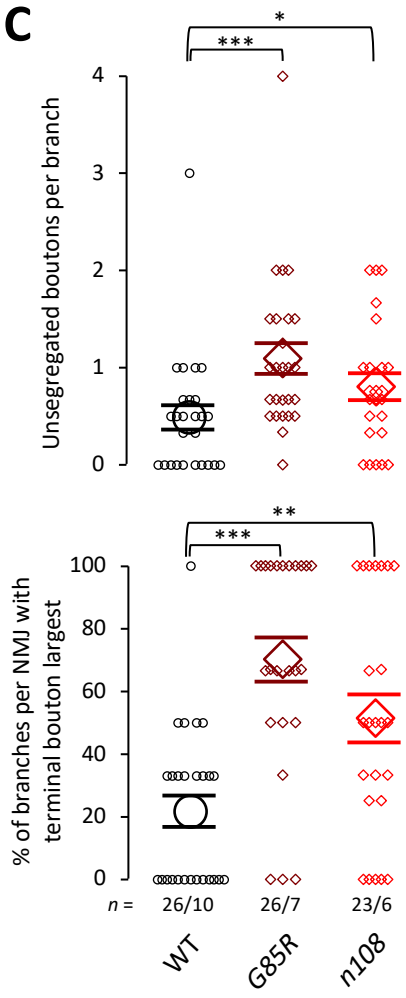
C
Unsegregated boutons per branch
% of branches per NMJ with terminal bouton largest
n =
26/10
26/7
23/6
WT
G85R
n108

Figure 2. Morphological defects in larval motor synapses of *Sod* mutants.

(A) Representative NMJ of larval muscles 4 (M4) and 13 (M13) from WT, Sod^{G85R}, and Sod^{n108}, immunostained with anti-HRP (neuronal membrane, green in merged image) and anti-Dlg (subsynaptic reticulum, red in merged image). Type Ib (tonic glutamatergic) branches were examined in both muscles, and type Is (phasic glutamatergic) branches were examined in M13. Is branches are distinguishable from Ib by their smaller size , and weaker anti-HRP and anti-Dlg immunostaining. Labels on the anti-HRP images indicate branch types. The much smaller type II boutons are also labeled, but were not studied. Select portions of the M4 and M13 images are magnified to show phenotypic incomplete bouton segregation (third row, green boxes) and terminal bouton enlargement (fourth row, gold boxes) in Sod^{G85R} and Sod^{n108}, compared to common WT variation. Note the "satellite" buds present on the magnified terminal bouton from Sod^{n108}. Scale bars in the upper left and lower left images are 10 μm.

(B) Per NMJ, number of branches (top) and synaptic boutons (bottom) of type Ib in M4 and M13, and type Is in M13. Branches are defined here as terminal processes composed of two or more synaptic boutons, distal of any bifurcations. Counts from larval abdominal segments 3, 4, and 5 are pooled. WT counts are plotted as black circles, Sod^{G85R} (*G85R*) as maroon diamonds, Sod^{n108} (*n108*) as red diamonds. Means are indicated by enlarged symbols, SEM by bars. * indicates $p < 0.05$, ** indicates $p < 0.01$, *** indicates $p < 0.001$ (Kruskal-Wallis test, rank-sum post hoc). *n* numbers (*n* of NMJ/*n* of larvae) are indicated above the genotype labels.

(C) Number of incompletely segregated (unsegregated) boutons per Ib branch per M4 NMJ (top), and percentage of Ib branches per M4 NMJ in which the terminal bouton was the largest after the last bifurcation. A bouton was described as incompletely segregated if the width of the narrowest point on the neck preceding it was greater than 80% of the width of the widest point on the bouton. The statistical parameters and their layout are identical to those of panel B.

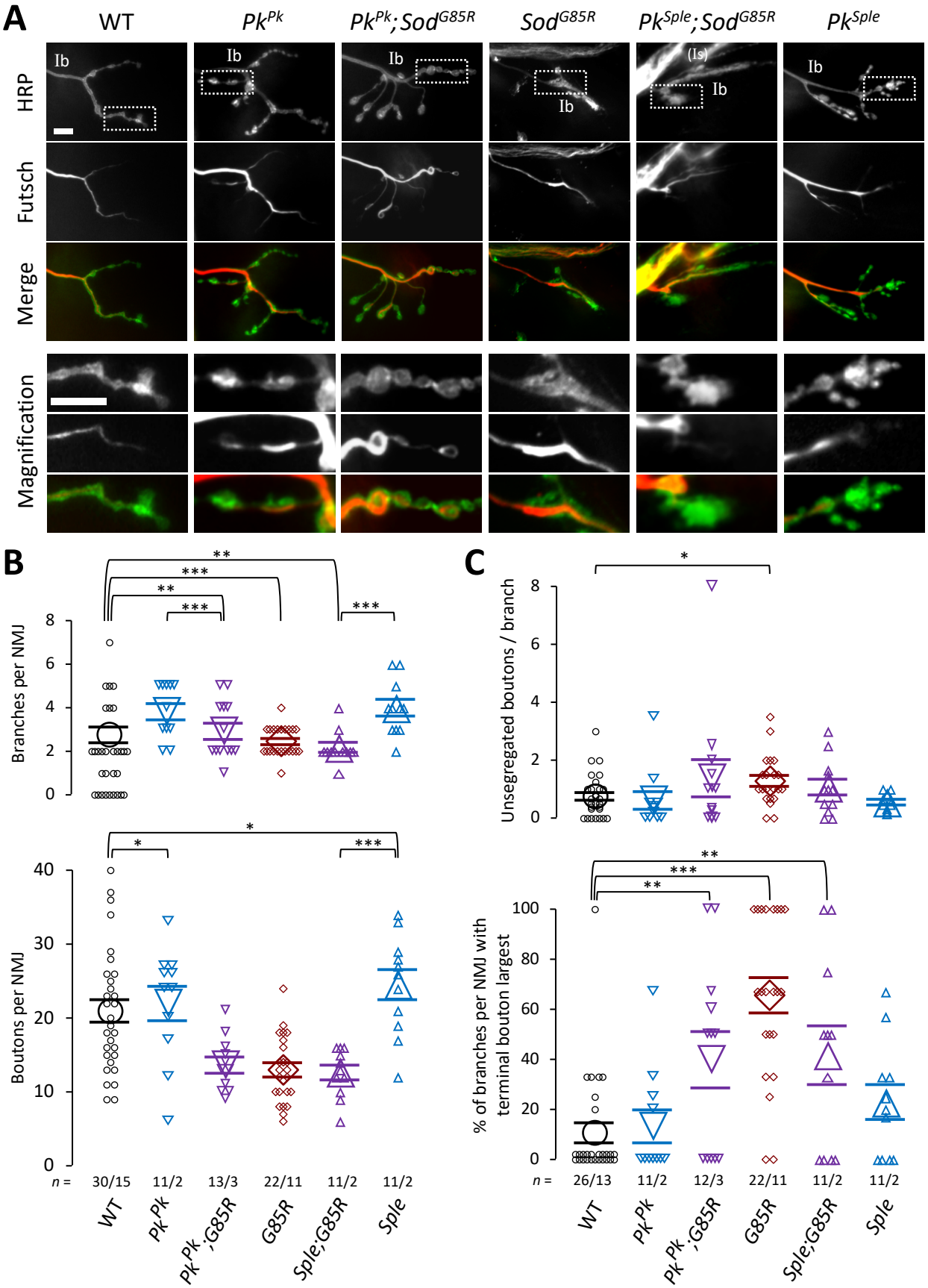
A
WT
Pk^Pk
Pk^Pk;Sod^G85R
Sod^G85R
Pk^Sple;Sod^G85R
Pk^Sple
HRP
Futsch
Merge
Magnification
Ib
(Is)
B
Branches per NMJ
Boutons per NMJ
C
Unsegregated boutons / branch
% of branches per NMJ with terminal bouton largest
n = 30/15 11/2 13/3 22/11 11/2 11/2
n = 26/13 11/2 12/3 22/11 11/2 11/2
WT
Pk^Pk
Pk^Pk;G85R
G85R
Sple;G85R
Sple

Figure 3. Larval NMJ morphology in double-mutants of *Pk* and *Sod*.

(A) Representative NMJ of larval muscle 4 (M4) (Ib branches) from WT, Sod^{G85R}, Pk^{Pk}, Pk^{Sple}, and the double mutants Pk^{Pk};Sod^{G85R} and Pk^{Sple};Sod^{G85R}. Presynaptic neuronal membrane is immunostained with anti-HRP (green in merged image) and the microtubule-associated protein Futsch is stained with the monoclonal AB 22C10 (red in merged image). Is branches are labeled where appropriate, but were not studied here. Select portions of the full-scale images are magnified to show characteristic bouton morphologies and cytoskeletal structures (bottom three rows). Note the greater and irregular intensities of Futsch staining in Sod^{G85R}, Pk^{Pk}, and Pk^{Pk};Sod^{G85R}, and the strongly stained "loop" structures in Pk^{Pk};Sod^{G85R}. Scale bars in the full-scale and magnified HRP images are 10 μm.

(B) Per M4 NMJ, number of type Ib branches (top) and synaptic boutons (bottom). Counts from larval abdominal segments 2, 4, and 6 are pooled. WT counts are plotted as black circles, Pk^{Pk} as blue inverted triangles, Pk^{Pk};Sod^{G85R} (Pk^{Pk};*G85R*) as purple inverted triangles, Sod^{G85R} (*G85R*) as maroon diamonds, Pk^{Sple};Sod^{G85R} (*Sple*;*G85R*) as purple upright triangles, (*Sple*) as blue upright triangles. Means are indicated by enlarged symbols, SEM by bars. * indicates $p < 0.05$, ** indicates $p < 0.01$, *** indicates $p < 0.001$ (Kruskal-Wallis test, rank-sum post hoc). *n* numbers (*n* of NMJ/*n* of larvae) are indicated above the genotype labels.

(C) Number of incompletely segregated (unsegregated) boutons per Ib branch per M4 NMJ (top), and percentage of Ib branches per M4 NMJ in which the terminal bouton was the largest after the last bifurcation. A bouton was described as incompletely segregated if the width of the narrowest point on the neck preceding it was greater than 80% of the width of the widest point on the bouton. The statistical parameters and their layout are identical to those of panel B.

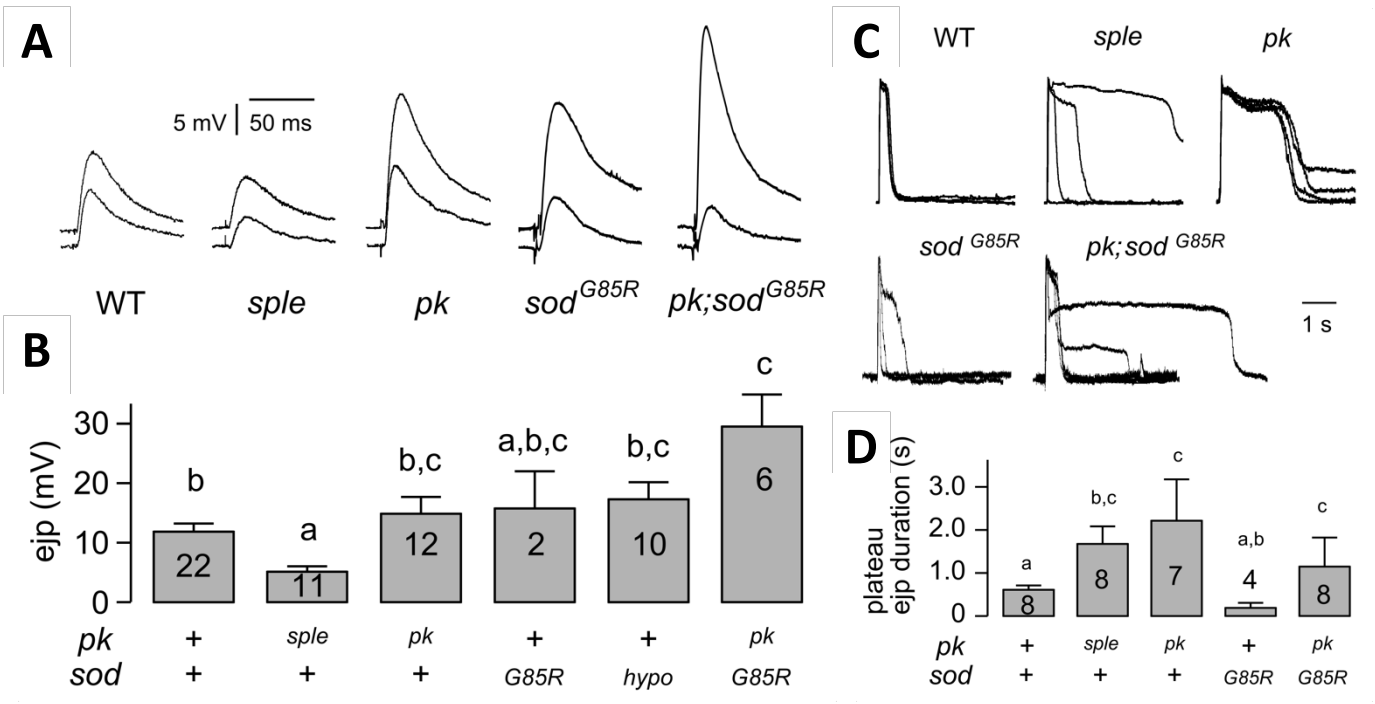
A
5 mV
50 ms
WT
sple
pk
sod G85R
pk;sod G85R
B
ejp (mV)
30
20
10
0
b
a
b,c
a,b,c
b,c
c
22
11
12
2
10
6
pk + sple pk + + pk
sod + + + G85R hypo G85R
C
WT
sple
pk
sod G85R
pk;sod G85R
1 s
D
plateau ejp duration (s)
3.0
2.0
1.0
0
a
b,c
c
a,b
c
8
8
7
4
8
pk + sple pk + pk
sod + + + G85R G85R

Figure 4. Whole-cell EJP recordings in *Sod* and *Pk*;*Sod*.

(A) Increased size and variability of excitatory junctional potentials (EJPs) from larval body wall muscles in pk;sodG85R. EJPs from two different muscles are shown as examples for each genotype.

(B) a, b, and c indicates that differences within the group is not significant ($p > 0.05$, One-way ANOVA). Error bars = SEM. Number of NMJs are indicated. Ejps were measured in HL3.1 saline containing 0.2 mM Ca2+.

(C) Excitability in pk and sod motor axon terminals. Synaptic transmission was induced by direct activation of the motor axon terminals by electrotonic stimulation in the presence of a Na+ channel blocker (TTX, 3 μM) and K+ channel blockers (4-AP, 200 μM and TEA, 20 mM). Under this condition, prolonged ejps supported by continuous transmitter release was recorded (see Text). Amplitude is normalized to the peak.

(D) The duration of plateaued ejps were prolonged and more variable among perparations in sple, pk, and pk;sodG85R. a, b, and c indicates that differences within the group is not significant ($p > 0.05$, F-test). Error bars = SEM. Number of NMJs are indicated.

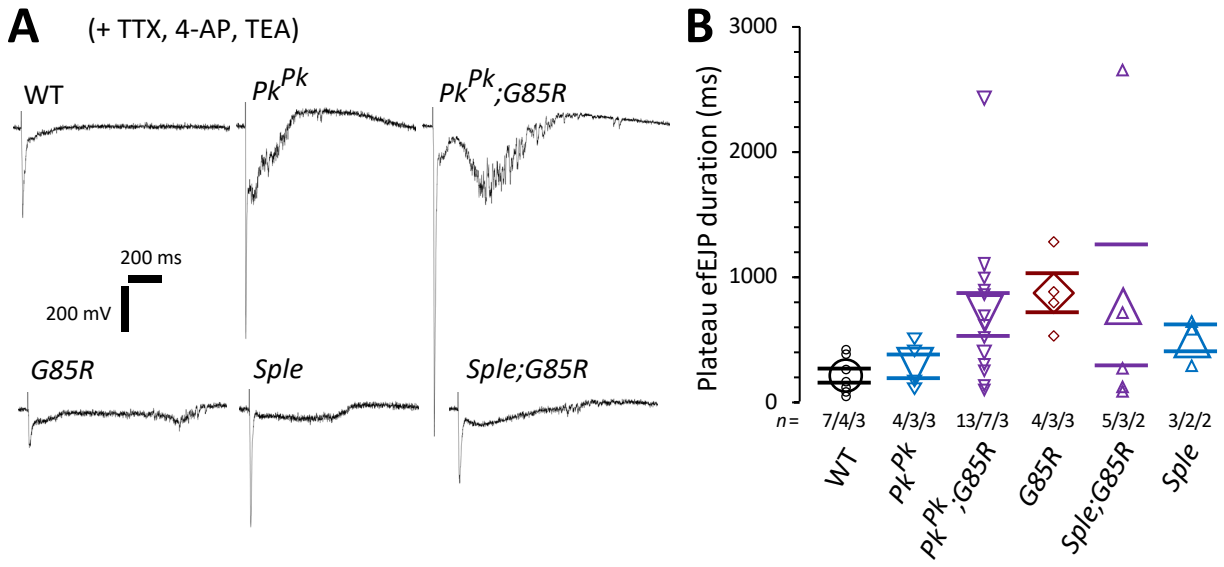
A
(+ TTX, 4-AP, TEA)
WT
Pk^Pk
Pk^Pk;G85R
200 ms
200 mV
G85R
Sple
Sple;G85R
B
Plateau efEJP duration (ms)
3000
2000
1000
0
n =
7/4/3
4/3/3
13/7/3
4/3/3
5/3/2
3/2/2
WT
Pk^Pk
Pk^Pk;G85R
G85R
Sple;G85R
Sple

Figure 5. Focal recording of plateau-like potentials induced at neuromuscular synapses by K^+ channel blockers.

(A) Sample focal recording (efEJP) traces from neuromuscular synapses of WT, Sod^{G85R}, Pk^{Pk}, Pk^{Sple}, Pk^{Pk};Sod^{G85R}, and Pk^{Sple};Sod^{G85R}, upon electrotonic stimulation after application of TTX (3 μM), 4-AP (200 μM), and TEA (20 mM). Recordings are from the NMJ of muscles 6 and 7, in larval segments A4 and A5. Each recording site contained between 1 and 4 boutons, and could contain a mixture of type Ib and type Is boutons. Note that trace amplitude is dependent on the variable seal resistance between the recording electrode and the NMJ. All artifacts have been truncated.

(B) Durations of plateau-like efEJP. At each recording site, a series of single stimulation pulses with incrementally increasing voltage was applied. The plotted plateau efEJP duration for each site is a measurement from the first plateau observed in the stimulation series. WT counts are plotted as black circles, Pk^{Pk} as blue inverted triangles, Pk^{Pk};Sod^{G85R} (*Pk*^{Pk};*G85R*) as purple inverted triangles, Sod^{G85R} (*G85R*) as maroon diamonds, Pk^{Sple};Sod^{G85R} (*Sple*;*G85R*) as purple upright triangles, Pk^{Sple} (*Sple*) as blue upright triangles. Means are indicated by enlarged symbols, SEM by bars. *n* numbers (*n* of recording sites/*n* of NMJ/*n* of larvae) are indicated above the genotype labels.

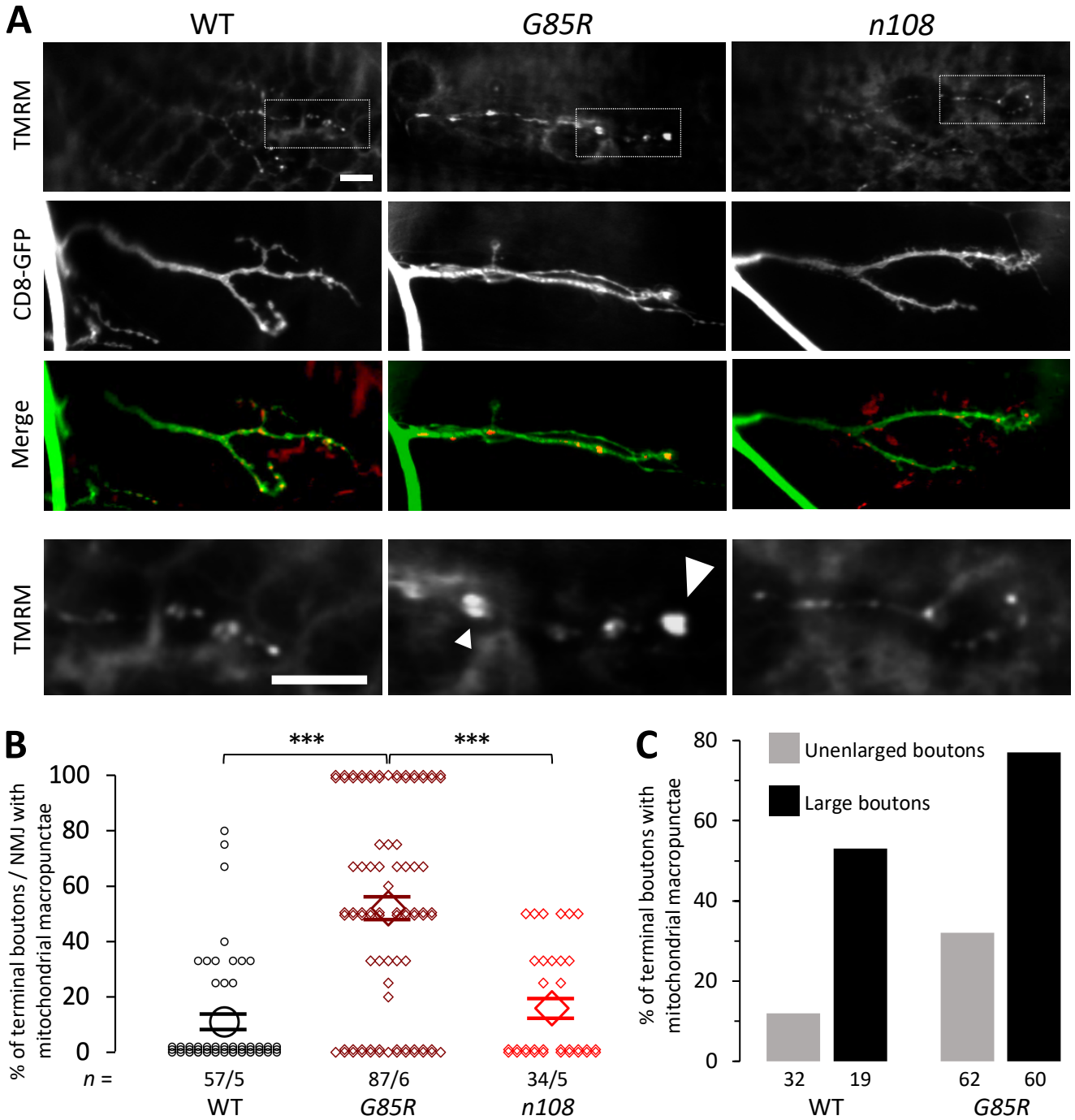
A
WT
G85R
n108
TMRM
CD8-GFP
Merge
TMRM
B
***
***
% of terminal boutons / NMJ with mitochondrial macropunctae
100
80
60
40
20
0
n =
57/5
87/6
34/5
WT
G85R
n108
C
% of terminal boutons with mitochondrial macropunctae
80
60
40
20
0
Unenlarged boutons
Large boutons
32
19
62
60
WT
G85R

Figure 6. Mitochondrial macropunctae in NMJ terminals of *Sod*^{G85R} larvae are frequently present in enlarged terminal boutons.

(A) Mitochondrial live tissue staining (TMRM, first row) in muscle 4 NMJ terminal branches in wild-type (WT), *Sod*^{G85R} (*G85R*), and *Sod*^{n108} (*n108*) larvae. The second row shows NMJ morphologies, visible with a presynaptic membrane-targeted GFP (CD8-GFP), expression of which was driven by a Gal4 construct (OK371). The third row shows overlays of the mitochondrial staining and presynaptic terminal images. The fourth row contains magnified portions of the whole-NMJ TMRM images (first row, white boxes). The larger white arrowhead indicates an *Sod*^{G85R} terminal bouton with a large, bright spot of mitochondrial staining, the smaller white arrowhead indicates bright staining in a non-terminal bouton. We describe these points of bright mitochondrial staining as "macropunctae". Scale bars in the upper left and lower left images are 10 μm.

(B) Percentages of branches per NMJ (muscle 4, type Ib boutons) in which staining revealed mitochondrial macropunctae in the terminal bouton in WT (black circles), *Sod*^{G85R} (maroon diamonds), *Sod*^{n108} (red diamonds). Counts from larval abdominal segments 2, 3, 4, 5, and 6 are pooled. Means are indicated by enlarged symbols, SEM by bars. *** indicates $p < 0.001$ (Kruskal-Wallis test, rank-sum post hoc). *n* numbers (*n* of NMJ/*n* of larvae) are indicated above the genotype labels.

(C) Percentages of large terminal boutons (enlarged compared to other boutons on the branch) (black) and unenlarged boutons (gray) in which staining revealed mitochondrial macropunctae, in WT and *Sod*^{G85R}. Bouton morphology was visible with visible with CD8-GFP. *n* number of boutons per category is indicated above each genotype label.

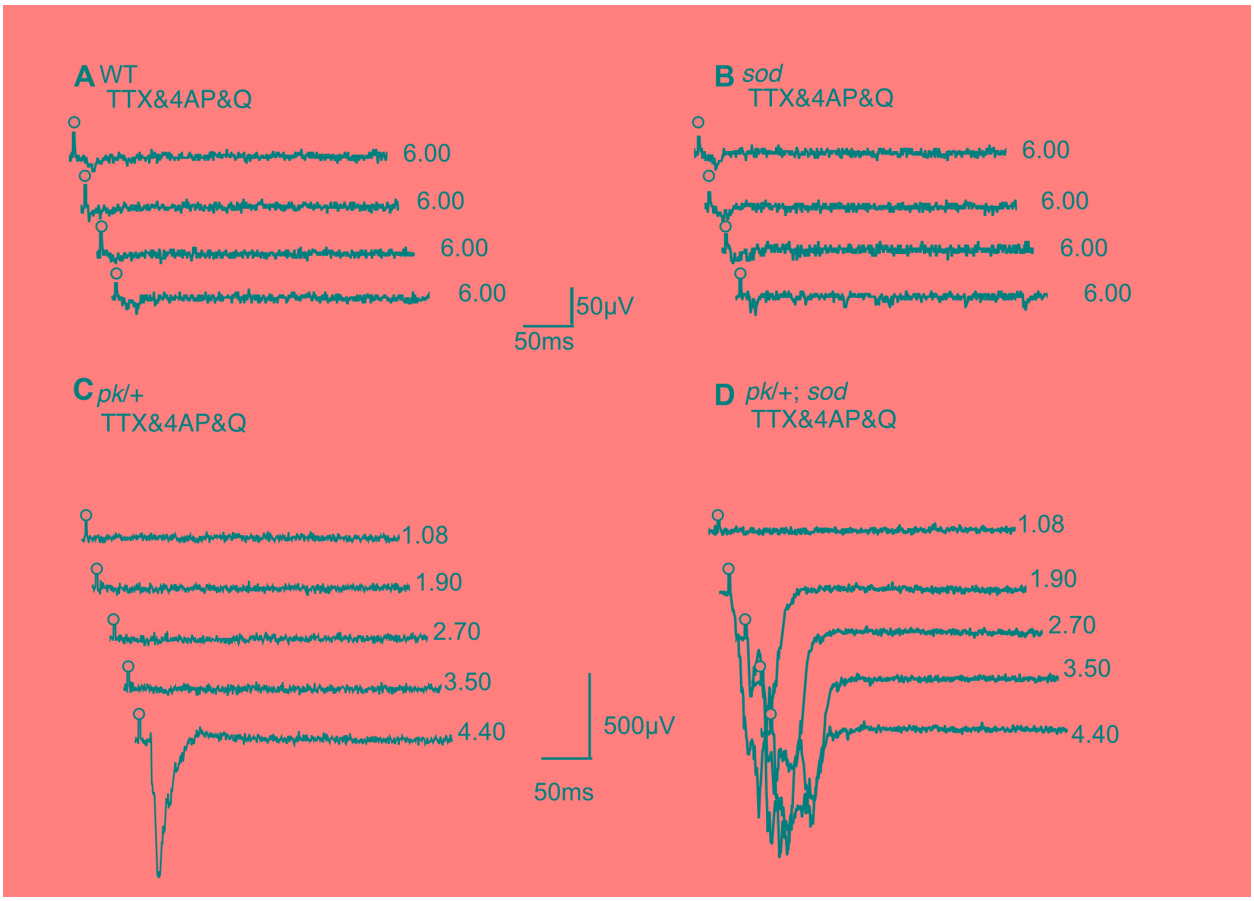
A WT
TTX&4AP&Q
6.00
6.00
6.00
6.00
50μV
50ms
B sod
TTX&4AP&Q
6.00
6.00
6.00
6.00
C pkl+
TTX&4AP&Q
1.08
1.90
2.70
3.50
4.40
500μV
50ms
D pkl+; sod
TTX&4AP&Q
1.08
1.90
2.70
3.50
4.40

Supplemental Figure 1. Focal recording examination of the excitability in *pk*^{pk} and *sod*^{n108} synaptic terminals.

Electrotonic stimuli (1 ms pulse duration) were applied to NMJ terminals at 0.1mM Ca2+ with Na^+ channel blockers (TTX, 3 μM) and K^+ channel blockers (4-AP, 200 μM and quinidine, 100 μM). Only type Ib boutons were recorded. (A) WT and (B) *sodn108* terminals quickly ran down after adding both 4-AP and quinidine and gave poor responses, whereas (C) *pk*^{pk} heterozygous (over CyO-GFP) and (D) *pk*^{pk}/CyO-GFP; *sodn108* displayed currents of striking amplitudes. Note that *pk*^{pk}/CyO-GFP; *sodn108* has lower stimulation voltage (in V, labeled on the side) threshold and wider response current width. All artifacts have been truncated. The circles above each trace indicate the locations of the artifacts induced by stimuli.

References

Aitken RJ, Krausz C. (2001) Oxidative stress, DNA damage, and the Y chromosome. *Reproduction* 122: 497-506.

Akbergenova Y, Bykhovskaia M. (2007) Synapsin maintains the reserve vesicle pool and spatial segregation of the recycling pool in *Drosophila* presynaptic boutons. *Brain Research* 1178: 52-64.

Albrecht SC, Barata AG, Großhans J, Teleman AA, Dick TP. (2011) In vivo mapping of hydrogen peroxide and oxidize glutathione reveals chemical and regional specificity of redox homeostasis. *Cell Metabolism* 14: 819-829.

Ali S, Jain SK, Abdulla M, Athar M. (1996) Paraquat induced DNA damage by reactive oxygen species. *Biochemistry and Molecular Biology International* 39(1): 63-67.

Altan O, Pabuccuoglu A, Altan A, Konyalioglu S, Bayraktar H. (2003) Effect of heat stress on oxidative stress, lipid peroxidation, and some stress parameters in broilers. *British Poultry Science* 44(4): 545-550.

Atwood HL, Govind CK, Wu CF. (1993) Differential ultrastructure of synaptic terminals on ventral longitudinal abdominal muscles in *Drosophila* larvae. *Journal of Neurobiology* 24(8):1008-1024.

Ayala GX, Tapia R. (2003) Expression of heat shock protein 70 induced by 4-aminopyridine through glutamate-mediated excitotoxic stress in rat hippocampus in vivo. *Neuropharmacology* 45: 649-660.

Baek MK, Kim KO, Kwon HJ, Kim YW, Woo JH, Kim DY. (2016) Age-related changes in antioxidative enzyme capacity in tongue of Fischer 344 rats. *Clinical and Experimental Otorhinolaryngology* 9(4): 352-357.

Bainbridge SP, Bownes M. (1981) Staging the metamorphosis of *Drosophila* melanogaster. *J. Embryol. exp. Morph.* 66: 57-80.

Bassuk AG, Wallace RH, Buhr A, ..., Slusarski DC, Berkovic SF, El-Shanti HI. (2008) A homozygous mutation in human PRICKLE1 causes an autosomal-recessive progressive myoclonus epilepsy-ataxia syndrome. *The American Journal of Human Genetics* 83: 572-581.

Beers DR, Ho BK, Siklos L, Alexianu ME, Mosier DR, Mohamed AH, ... Appel SH. (2001) Parvalbumin overexpression alters immune-mediated increases in intracellular calcium, and delays disease onset in a transgenic model of familial amyotrophic lateral sclerosis. *Journal of Neurochemistry* 79: 499-509.

Berlett BS, Stadtman ER. (1997) Protein Oxidation in Aging, Disease, and Oxidative Stress. *The Journal of Biological Chemistry* 272(33): 20313-20316.

Bilsland LG, Sahai E, Kelly G, Golding M, Greensmith L, Schiavo G. (2010) Deficits in axonal transport precede ALS symptoms in vivo. *Proc Natl Acad Sci* 107(47): 20523-20528.

Block ML, Calderón-Garcidueñas L. (2009) Air pollution: mechanisms of neuroinflammation and CNS disease. *Trends in Neurosciences* 32(9): 506-516.

Brand AH, Perrimon N. (1993) Targeted gene expression as a means of altering cell fates and generating dominant phenotypes. *Development* 118:401-415.

Budnik V, Koh YH, Guan B, Hartmann B, Hough C, Woods D, Gorczyca M. (1996) Regulation of synapse structure and function by the *Drosophila* tumor suppressor gene *dlg*. *Neuron* 17: 627-640.

Campbell SH, Hilliker AJ, Phillips JP. (1985) Cytogenetic analysis of the *cSOD* microregion in *Drosophila melanogaster*. *Genetics* 112: 205-215.

Chen Q, Vasquez EJ, Moghaddas S, Hoppel CL, Lesnefsky EJ. (2003) Production of reactive oxygen species by mitochondria. *The Journal of Biological Chemistry* 278(38): 36027-36031.

Chen Y, Cohen TJ. (2019) Aggregation of the nucleic acid– binding protein TDP-43 occurs via distinct routes that are coordinated with stress granule formation. *J Biol Chem* 294(10): 3696-3706.

Chowdhury SR, Djordjevic J, Albensi BC, Fernyhough P. (2016) Simultaneous evaluation of substrate-dependent oxygen consumption rates and mitochondrial membrane potential by TMRM and safranin in cortical mitochondria. *Biosci Rep* 36: e00286

Culotta & Daly. (2013) Manganese Complexes: Diverse Metabolic Routes to Oxidative Stress Resistance in Prokaryotes and Yeast. *Antioxidants and Redox Signaling* 19(9): 933-944.

De Vos KJ, Chapman AL, Tennant ME, Manser C, Tudor EL, ... Grierson AJ. (2007) Familial amyotrophic lateral sclerosis-linked SOD1 mutants perturb fast axonal transport to reduce axonal mitochondria content. *Hum Mol Genet* 16(22): 2720-2728.

Dhalla NS, Temsah RM, Netticadan, T. (2000) Role of oxidative stress in cardiovascular diseases. *Journal of Hypertension*, 18(6): 655-673.

Ehaideb SN, Iyengar A, Ueda A, Iacobucci GJ, Cranston C, Bassuk AG, Gubb D, Axelrod JD, Gunawardena S, Wu CF, Manak RJ. (2014) *prickle* modulates microtubule

polarity and axonal transport to ameliorate seizures in flies. *Proc. Natl. Acad. Sci. USA* 111(30): 11187-11192.

Ehaideb SN, Wignall EA, Kasuya J, Evans WH, Iyengar A, Koerselman HL, Lilienthal AJ, Bassuk AG, Kitamoto T, Manak RJ. (2016) Mutation of orthologous prickle genes causes a similar epilepsy syndrome in flies and humans. *Annals of Clinical and Translational Neurology* 3 (9): 695-707.

Estes PS, Roos J, van der Bliek A, Kelly RB, Krishnan KS, Ramaswami M. (1996) Traffic of Dynamin within individual *Drosophila* synaptic boutons relative to compartment-specific markers *J. Neurosci.* 1996 16(17): 5443-5456.

Fatt P, Katz B. (1951) An analysis of the end-plate potential recorded with an intra-cellular electrode. *J. Physiol.* 115: 320-370.

Fatt P, Katz B. (1952) Spontaneous subthreshold activity at motor nerve endings. *J. Physiol.* 117: 109-128.

Feng Y, Ueda A, Wu CF. (2004) A modified minimal hemolymph-like solution, HL3. 1, for physiological recordings at the neuromuscular junctions of normal and mutant Drosophila larvae. *Journal of Neurogenetics*, 18(2): 377-402.

Floryk D, Houštěk J. (1999) Tetramethyl rhodamine methyl ester (TMRM) is suitable for cytofluorometric measurements of mitochondrial membrane potential in cells treated with digitonin. *Bioscience Reports* 19(1): 27-34.

Forsberg K, Andersen PM, Marklund SL, Brannstrom T. (2011) Glial nuclear aggregates of superoxide dismutase-1 are regularly present in patients with amyotrophic lateral sclerosis. *Acta Neuropathol* 121: 623-634.

Frankel, A., & Brousseau, G. (1968). Drosophila medium that does not require dried yeast. *Drosophila Information Service* 43, 184.

Fujita SC, Zipursky SL, Benzer S, Ferrús, Shotwell SL. (1982) Monoclonal antibodies against the *Drosophila* nervous system. *Proc. Natl. Acad. Sci USA* 79: 7929-7933.

Galvin (2017) The path to specialist multidisciplinary care in amyotrophic lateral sclerosis: A population- based study of consultations, interventions and costs. *PLoS ONE* 12(6): e0178796.

Ganetzky B, Wu CF. (1982) *Drosophila* mutants with opposing effects on nerve excitability: Genetic and spatial interactions in repetitive firing. *Journal of Neurophysiology* 47(3): 501-514.

Ganetzky B, Wu CF. (1983) Neurogenetic analysis of potassium currents in *Drosophila*: Synergistic effects on neuromuscular transmission in double mutants. *Journal of Neurogenetics* 1: 17-28.

Guegan S, Prezedborski C. (2003) Programmed cell death in amyotrophic lateral sclerosis. *J Clin Invest* 111:153-161.

Giorgi C, Marchi S, Pinton P. (2018) The machineries, regulation and cellular functions of mitochondrial calcium. *Nature Reviews: Molecular Cell Biology* 19: 713-730.

Gubb D, García-Bellido A. (1982) A genetic analysis of the determination of cuticular polarity during development in *Drosophila melanogaster*. *J. Embryol. exp. Morph.* 68: 337-57.

Gubb D, Green C, Huen D, Coulson D, Johnson G, Tree D, Collier S, Roote J. (1999) The balance between isoforms of the Prickle LIM domain protein is critical for planar polarity in *Drosophila* imaginal discs. *Genes & Development* 13: 2315-2327.

Gray RS, Roszko I, Solnica-Krezel L. (2011) Planar cell polarity: coordinating morphogenetic cell behaviors with embryonic polarity. *Developmental Cell* 21: July 19, 2011.

Hardiman O, van den Berg LH, Kiernan MC. (2011) Clinical diagnosis and management of amyotrophic lateral sclerosis. *Nature Reviews: Neurology* 7: 639-649.

Harman D. (1956) Aging: A theory based on free radical and radiation chemistry. *Journal of Gerontology* 11(3): 298-300.

Harris KP, Littleton T. (2015) Transmission, development, and plasticity of synapses. *Genetics* 201: 345-375.

Heitzler P, Coulson D, Saenz-Robles M-T, Ashburner M, Roote J, Simpson P, Gubb D. (1993) Genetic and cytogenetic analysis of the 43A-E region containing the segment polarity gene *costa* and the cellular polarity genes *prickle* and *spiny-legs* in *Drosophila melanogaster*. *Genetics* 135: 105-115.

Held A, Major P, Sahin A, Reenan RA, Lipscombe D, Wharton KA. (2019) Circuit dysfunction in SOD1-ALS model first detected in sensory feedback prior to motor neuron degeneration is alleviated by BMP signaling. *Neurobiology of Disease* 39(12): 2347-2364.

Hummel T, Krukkert K, Roos J, Davis G, Klämbt C. (2000) *Drosophila* Futsch/22C10 is a MAP1B-like protein required for dendritic and axonal development. *Neuron* 26: 357-370.

Jan LY, Jan YN. (1976a) Properties of the larval neuromuscular junction in *Drosophila melanogaster*. *J. Physiol.* 262: 189-214.

Jan LY, Jan YN. (1976b) L-glutamate as an excitatory transmitter at the *Drosophila* larval neuromuscular junction. *J. Physiol.* 262: 215-236.

Jan YN, Jan LY, Dennis MJ. (1977) Two mutations of synaptic transmission in *Drosophila. Proc. R. Soc. Lond. B.* 198: 87-108.

Jan LY, Jan YN. (1982) Antibodies to horseradish peroxidase as specific neuronal markers in *Drosophila* and in grasshopper embryos. *Proc. Natl. Acad. Sci. USA* 79: 2700-2704.

Kannan K, Jain SK. (2000) Oxidative stress and apoptosis. *Pathophysiology* 7(27) 153-163.

Katz B, Miledi R. (1967a) A study of synaptic transmission in the absence of nerve impulses. *J. Physiol.* 192: 407-436.

Katz B, Miledi R. (1967b) Tetrodotoxin and neuromuscular transmission. *Proceedings of the Royal Society B* 167 (1006): 8-22.

Kawasaki F, Collins SC, Ordway RW. (2002) Synaptic calcium-channel function in *Drosophila*: Analysis and transformation rescue of temperature-sensitive paralytic and lethal mutations of *cacophony*. 22(14): 5856-5864.

Klagges BRE, Heimbeck G, Godenschwege TA, Hofbauer A, Pflugfelder GO, Reifegerste R, Reisch D, Schaupp M, Buchner S, Buchner E. (1996) Invertebrate synapsins: A single gene codes for several isoforms in *Drosophila*. *J. Neurosci.* 16(10): 3154-3165.

Kurdyak P, Atwood HL, Stewart BA, Wu CF. (1994) Differential physiology and morphology of motor axons to ventral longitudinal muscles in larval *Drosophila. The Journal of Comparative Neurology* 350: 463-472.

Kurosaka A, Yano A, Itoh N, Kuroda Y, Nakagawa T, Kawasaki T. (1991) The structure of a neural specific carbohydrate epitope of horseradish peroxidase antiserum. *the Journal of Biological Chemistry* 266(7): 4168-4172.

Landis G, Shen J, Tower J. (2012) Gene expression changes in response to again compared to heat stress, oxidative stress and ionizing radiation in *Drosophila melanogaster*. *Aging* 4(11): 768-789.

Lee T, Luo L. (2001) Mosaic analysis with a repressible cell marker (MARCM) for *Drosophila* neural development. *Trends in Neurosciences* 24(5): 251-254.

Lee J, Ueda A, Wu CF (2014) Distinct roles of *Drosophila cacophony* and *Dmca1D* Ca2+ channels in synaptic homeostasis: Genetic interactions with *slowpoke* Ca2+-

activated BK channels in presynaptic excitability and postsynaptic response. *Dev. Neurobiol.* 141: 4548-4557.

Lee J, Wu CF. (2010) Orchestration of Stepwise Synaptic Growth by K+ and Ca2+ Channels in *Drosophila*. *J. Neurosci.* 30(47): 15921-15833.

Liguori I, Russo G, Curcio F, Bulli G, Aran L, Della-Morte D, Gargiulo G, ... Abete P. (2018) Oxidative stress, aging, and diseases. *Clinical interventions in Aging* 13: 757-772.

Lin CLG, Bristol LA, Jin L, Dykes-Hoberg M, Crawford T, Clawson L, Rothstein JD. (1998) Aberrant RNA processing in a neurodegenerative disease: the cause for absent EAAT2, a glutamate transporter, in amyotrophic lateral sclerosis. *Neuron* 20: 589-602.

Lin YY, Gubb D. (2009) Molecular dissection of *Drosophila* Prickle isoforms distinguishes their essential and overlapping roles in planar cell polarity. *Developmental Biology* 325: 386-399.

Lushchak, V. I. (2014) Free radicals, reactive oxygen species, oxidative stress and its classification. *Chem-Biol Interact* 224: 164–175.

MacAskill AF, Kittler JT. (2009) Control of mitochondrial transport and localization in neurons. *Trends in Cell Biology* 20(2): 102-112.

Mackenzie IRA, Rademakers R. (2008) Aberrant RNA processing in a neurodegenerative disease: the cause for absent EAAT2, a glutamate transporter, in amyotrophic lateral sclerosis. *Curr Opin Neurol* 21(6): 693-700.

Mahr A, Aberle H. (2006) The expression pattern of the *Drosophila* vesicular glutamate transporter: A marker protein for motoneurons and glutamatergic centers in the brain. *Gene Expression Patterns* 6: 299-309.

Massaad CA, Klann E. (2011) Reactive Oxygen Species in the Regulation of Synaptic Plasticity and Memory. *Antioxidants and Redox Signaling* 14(10): 2013-2054.

Mates, J. M., Perez-Gomez, C., de Castro, IN. (1999). Antioxidant enzymes and human diseases. *Clinical Biochemistry* 32(8): 595-603.

McCord JM, Fridovich I. (1969) Superoxide dismutase: An enzymatic function for erythrocuprein (hemocuprein). *J. Biol. Chem.* 244: 6049-6055.

Mei X, Wu S, Bassuk AG, Slusarski DC. (2013) Mechanisms of *prickle1a* function in zebrafish epilepsy and retinal neurogenesis. *Disease Models & Mechanisms* 6: 679-688.

200 Milton VJ, Jarrett HE, Gowers K, Chalak S, Briggs L, Robinson IM, Sweeney ST. (2011)
201 Oxidative stress induces overgrowth of the *Drosophila* neuromuscular junction. *Proc*
202 *Natl Acad Sci* 108(42): 17521-17526.
203 Mondola P, Damiano S, Sasso A, Santillo M. (2016) The Cu,Zn superoxide dismutase: not
204 only a dismutase enzyme. *Front Physiol* 7: 594.
205 Morfini GA, Bosco DA, Brown H, Gatto R, Kaminska A, Song Y, Molla L, Baker L,
206 Marangoni MN, Berth S, Tavassoli E, Bagnato C, Tiwari A, Hayward LJ, Pigino GF,
207 Watterson DM, Huang CF, Banker G, Brown RH Jr, Brady ST. (2013) Inhibition of
208 fast axonal transport by pathogenic SOD1 involves activation of p38 MAP kinase.
209 *PLOS ONE* 8(6): e65235.
210 Osking Z, Ayers JI, Hildebrandt R, Skruber K, Brown H, Ryu D, ... Vitriol EA. (2019) ALS-
211 linked SOD1 mutants enhance neurite outgrowth and branching in adult motor
212 neurons. *iScience* 11: 294-304.
213 Ott M, Gogvadze V, Orrenius S, Zhivotozsky B. (2007) Mitochondria, oxidative stress and
214 cell death. *Apoptosis* 12: 913-922.
215 Paemka L, Mahajan VB, Skeie JM, ..., Carvill GL, Manak RJ, Bassuk AG. (2013)
216 PRICKLE1 interaction with SYNAPSIN I reveals a role in autism spectrum disorders.
217 *PLOS ONE* 8 (12): e80737.
218 Paniker NV, Srivastava SK, Beutler E. (1970) Glutathione metabolism of the red cells effect
219 of glutathione reductase deficiency on the stimulation of hexose monophosphate
220 shunt under oxidative stress. *Biochim. Biophys. Acta* 215: 456-460.
221 Parnas D, Haghighi P, Fetter RD, Kim SW, Goodman CS. (2001) Regulation of
222 postsynaptic structure and protein localization by the rho-type guanine nucleotide
223 exchange factor dPix. *Neuron* 32: 415-424.
224 Patel A, Lee HO, Jawerth L, Maharana S, Jahnel M, Hein MY, Stoynov S, ... Alberti S.
225 (2015) A liquid-to-solid phase transition of the ALS protein FUS accelerated by
226 disease mutation. *Cell* 162, 1066-1077.
227 Peng IF, Berke BA, Zhu Y, Lee WH, Chen W, Wu CF. (2007) Temperature-dependent
228 developmental plasticity of *Drosophila* neurons: Cell-autonomous roles of
229 membrane excitability, Ca2+ influx, and cAMP signaling. *The Journal of*
230 *Neuroscience* 27(46): 12611-12622.
231 Perry JJP, Shin DS, Getzoff ED, Tainer JA. (2010) The structural biochemistry of the
232 superoxide dismutases. *Biochim Biophys Acta* 1804(2): 245-262.

Phillips JP, Campbell SD, Michaud D, Charbonneau M, Hilliker, AJ. (1989) Null mutation of copper/zinc superoxide dismutase in Drosophila confers hypersensitivity to paraquat and reduced longevity. *Proc Natl Acad Sci* 86(8): 2761-2765.

Renger JJ, Ueda A, Atwood HL, Govind CK, Wu CF. (2000) Role of cAMP cascade in synaptic stability and plasticity: Ultrastructural and physiological analyses of individual synaptic boutons in *Drosophila* memory mutants. *J. Neurosci.* 20(11): 3980-3992.

Rosen DR, Siddique T, Patterson D, Figlewicz DA, Sapp P, Hentati A, ... Brown RH Jr. (1993) Mutations in Cu/Zn superoxide dismutase gene are associated with familial amyotrophic lateral sclerosis. *Nature* 362: 59-62.

Rowland LP, Shneider NA. (2001). Amyotrophic lateral sclerosis. *The New England Journal of Medicine* 344(22): 1688-1700.

Ruan, H., & Wu, C. F. (2008). Social interaction-mediated lifespan extension of *Drosophila* Cu/Zn superoxide dismutase mutants. *Proc Natl Acad Sci* 105(21): 7506-7510.

Saccon RA, Bunton-Stasyshyn RKA, Fisher EMC, Fratta P. (2013) Is SOD1 loss of function involved in amyotrophic lateral sclerosis. *Brain* 136: 2342-2358.

Şahin A, Held A, Bredvik K, Major P, Achilli TM, Kerson, AG, ... Reenan, R. (2017). Human SOD1 ALS mutations in a *Drosophila* knock-in model cause severe phenotypes and reveal dosage-sensitive gain- and loss-of-function components. *Genetics* 205(2): 707-723.

Salińska E, Danysz W, Łazarexicz JW. (2005) The role of excitotoxicity in neurodegeneration. *Folia Neuropathol* 43(4): 322-339.

Sies H. (1997) Oxidative Stress: Oxidants and Antioxidants (Physiological Society Symposium: Impaired endothelial and smooth muscle cell function in oxidative stress). *Experimental Physiology* 82: 291-295.

Singh S, Wu CF. (1999) Ionic currents in larval muscles of *Drosophila. International Review of Neurobiology* 43: 191-220.

Smith EF, Shaw PJ, De Vos KJ. (2017) The role of mitochondria in amyotrophic lateral sclerosis. *Neurosci Lett* 710: 132933.

Smith LA, Wang XJ, Peixoto AA, Neumann EK, Hall LM, Hall JC. (1996) A *Drosophila* calcium channel α1 subunit gene maps to a genetic locus associated with behavioral and visual defects. *J. Neurosci.* 16(24): 7868-7879.

265 Sørensen JG, Nielsen MM, Kruhøffer M, Justesen J, Loeschcke V. (2005) Full genome
266 gene expression analysis of the heat stress response in *Drosophila melanogaster*.
267 *Cell Stress Chaperones*. 10(4): 312-328.
268 Sosa V, Moliné T, Somoza R, Paciucci R, Kondoh H, Lleonart ME. (2013) Oxidative stress
269 and cancer: An overview. *Ageing Research Reviews* 12: 376-390.
270 Stewart BA, Atwood HL, Renger JJ, Wang J, Wu CF. (1994) Improved stability of
271 *Drosophila* larval neuromuscular preparations in haemolymph-like physiological
272 solutions. *J Comp Physiol A* 175: 179-191.
273 Tang H, Tian E, Liu C, Wang Q, Deng H. (2013) Oxidative stress induces monocyte
274 necrosis with enrichment of cell-bound albumin and overexpression of endoplasmic
275 reticulum and mitochondrial chaperones. *PLoS ONE* 8(3): e59610.
276 Tao H, Manak RJ, Sowers L, ..., Wemmie J, Ueno N, Bassuk AG. (2011) Mutations in
277 Prickle orthologs cause seizures in flies, mice, and humans. *The American Journal*
278 *of Human Genetics* 88: 138-149.
279 Thannickal VJ, Fanburg BL. (2000) Reactive oxygen species in cell signaling. *Am J Physiol*
280 *Lung Cell Mol Physiol* 279: L1005-L1028.
281 Torroja L, Packard M, Gorczyca M, White K, Budnik V. (1999) The *Drosophila* β-amyloid
282 precursor protein homolog promotes synapse differentiation at the neuromuscular
283 junction. *The Journal of Neuroscience* 19(18): 7793-7803.
284 Tree DRP, Shulman JM, Rousset R, Scott MP, Gubb D, Axelrod JD. (2002) Prickle
285 mediates feedback amplification to generate asymmetric planar cell polarity
286 signaling. *Cell* 109: 371-381.
287 Trotti D, Rolfs A, Danbolt NC, Brown RH Jr, Hediger MA. (1999) SOD1 mutants linked to
288 amyotrophic lateral sclerosis selectively inactivate a glial glutamate transporter.
289 *Nature Neuroscience* 2(5): 427-433.
290 Tsang CK, Liu Y, Thomas J, Zhang Y, Zheng XFS. (2015) Superoxide dismutase 1 acts as
291 a nuclear transcription factor to regulate oxidative stress resistance. *Nat Commun*
292 5:3446.
293 Ueda A, Wu CF. (2006) Distinct frequency-dependent regulation of nerve terminal
294 excitability and synaptic transmission by I_A and I_K potassium channels revealed by
295 *Drosophila Shaker* and *Shab* mutations. *The Journal of Neuroscience* 26(23): 6238-
296 6248.

297 Ueda A, Wu CF. (2008) Effects of *Hyperkinetic*, a beta-subunit of *Shaker* voltage-
298 dependent K+ channels, on the oxidation state of presynaptic nerve terminals. *J*
299 *Neurogenet* 22(2): 1-13.
300 Ueda A, Wu CF. (2009) Role of *rut* adenylyl cyclase in the ensemble regulation of
301 presynaptic terminal excitability: Reduced synaptic strength and precision in a
302 *Drosophila* memory mutant. *J Neurogenet* 23: 185-199.
303 Uttara B, Singh AV, Zamboni P, Mahajan RT. (2009) Oxidative stress and
304 neurodegenerative diseases: a review of upstream and downstream antioxidant
305 therapeutic options. *Current Neuropharmacology* 7: 65-74.
306 Van Raamsdonk JM, Hekimi S. (2012) Superoxide dismutase is dispensable for normal
307 animal lifespan. *Proc Natl Acad Sci* 109(15): 5785-5790.
308 Vande Velde C, McDonald KK, Boukhedimi Y, ... Cleveland DW. (2011) Misfolded SOD1
309 Associated with Motor Neuron Mitochondria Alters Mitochondrial Shape and
310 Distribution Prior to Clinical Onset. *PLoS ONE* 6(7): e22031.
311 Vasin A, Zueva L, Torrez C, Volfson A, Littleton JT, Bykhovskaia M. (2014) Synapsin
312 regulates activity-dependent outgrowth of synaptic boutons at the *Drosophila*
313 neuromuscular junction. *J. Neurosci.* 34(32): 10554-10563.
314 Wang J, Farr GW, Zeiss CJ, Rodriguez-Gil DJ, Wilson JH, ... Horwich AL. (2008)
315 Progressive aggregation despite chaperone associations of a mutant SOD1-YFP in
316 transgenic mice that develop ALS. *Proc Natl Acad Sci* 106(5): 1392-1897.
317 Wang J, Farr GW, Hall DH, Li F, Furtak K, Dreier L, ... Horwich AL. (2009) An ALS-Linked
318 Mutant SOD1 Produces a Locomotor Defect Associated with Aggregation and
319 Synaptic Dysfunction When Expressed in Neurons of Caenorhabditis elegans. *PLoS*
320 *Genetics* 5(1): e1000350.
321 Wang JW, Humphreys JM, Phillips JP, Hilliker AJ, Wu CF. (2000) A novel leg-shaking
322 *Drosophila* mutant defective in a voltage-gated K^+ current and hypersensitive to
323 reactive oxygen species. *Journal of Neuroscience* 20(16): 5958-5964.
324 Wu CF, Ganetzky B, Jan LY, Jan YN, Benzer S. (1978) A *Drosophila* mutant with a
325 temperature-sensitive block in nerve conduction. *Proc Natl Acad Sci USA* 75(8):
326 4047-4051.
327 Xia R, Liu Y, Yang L, Gal J, Zhu H, Jia J. (2012) Motor neuron apoptosis and
328 neuromuscular junction perturbation are prominent features in a *Drosophila* model of
329 Fus-mediated ALS. *Molecular Neurodegeneration* 7:10.

330 Xing X, Wu CF. (2018a) Unraveling synaptic GCaMP signals: Differential excitability and
331 clearance mechanisms underlying distinct Ca^{2+} dynamics in tonic and phasic
332 excitatory, and aminergic modulatory motor terminals in *Drosophila*. *eNeuro* 5(1):
333 e0362-17.2018 1-28
334 Xing X, Wu CF. (2018b) Inter-relationships among physical dimensions, distal–proximal
335 rank orders, and basal GCaMP fluorescence levels in Ca^{2+} imaging of functionally
336 distinct synaptic boutons at *Drosophila* neuromuscular junctions. *J Neurogenet*
337 32(3): 195-208.
338 Zarei S, Carr K, Reiley L, Diaz K, Guerra O, Fernandez Altamirano P, ... Chinea A. (2015) A
339 comprehensive review of amyotrophic lateral sclerosis. *Surgical Neurology*
340 *International* 6:171.
341 Zhang Y, Liu Y, Walsh M, Bokov A, Ikeno Y, Jang YC, Perez VI, ... Richardson A. (2016)
342 Liver specific expression of Cu/ZnSOD extends the lifespan of *Sod1* null mice. *Mech*
343 *Ageing Dev* 154:1-8.
344 Zhong Y, Budnik V, Wu CF. (1992) Synaptic plasticity in *Drosophila* memory and
345 hyperexcitable mutants: role of cAMP cascade. *J Neurosci* 12(2): 644-651.
346 Zhong Y, Wu CF. (1991) Altered synaptic plasticity in Drosophila memory mutants with a
347 defective cyclic AMP cascade. *Science* 251(4990): 198-201.
348 Zipursky SL, Venkatesh TR, Teplow DB, Benzer S. (1984) Neuronal development in the
349 *Drosophila* retina: Monoclonal antibodies as molecular probes. *Cell* 36: 15-26.